ChemComm

ROYAL SOCIETY OF CHEMISTRY

COMMUNICATION

View Article Online
View Journal

Cite this: DOI: 10.1039/d6cc01757f

Received 23rd March 2026,
Accepted 28th May 2026

DOI: 10.1039/d6cc01757f

rsc.li/chemcomm

From RRDE to GDE: loading-dependent H_2O_2 selectivity loss in Sn- and Sb-N-C catalysts

Marco Mazzucato, Riccardo Marinello and Christian Durante *

Electrochemical H_2O_2 synthesis using Sn- and Sb-based single-site catalysts reveals that selectivity observed by RRDE can be lost in GDEs at higher catalyst loadings, highlighting the need for caution when translating model measurements to device-relevant conditions.

The use of water as a hydrogen source for the synthesis of useful chemicals is of growing interest,[1] particularly in processes where H_2 comes from steam reforming. Electrochemical oxygen reduction reaction (ORR) *via* a 2-electron pathway (2e-ORR) offers an interesting alternative to the consolidated anthraquinone process by simultaneously eliminating the need for gaseous hydrogen and organic solvents, and allowing more decentralized production.[2,3] The development of efficient and selective electrocatalysts is the first crucial step for enabling the practical implementation of this approach. In particular, catalysts capable of promoting the 2e-ORR pathway toward H_2O_2 while suppressing the competing four-electron reduction to water are highly desirable.[3,4] Historically promising catalysts for H_2O_2 production were based on Pd, Au, and Hg, with all the related issues (cost, availability, and safety), but recent interest has shifted toward cheaper metal-based catalysts and metal-free catalysts.[3,5] For this reason, a reliable evaluation of catalytic activity and selectivity is essential during the early stages of catalyst development. Electrochemical screening methods at the laboratory scale play a key role in identifying promising materials and understanding their intrinsic behavior under controlled conditions; in other words, they cannot forbear quick evaluation of the activity and selectivity of the electrocatalysts. For this reason, testing in a rotating ring disk electrode (RRDE) is a well-consolidated practice to simultaneously probe the ability to reduce O_2 (activity) and the effectiveness of following the desired pathway (selectivity). This setup is highly versatile across a wide pH range and in several electrolytes,[6–8] thanks to the possibility of preparing thin films on a glassy carbon (GC) electrode, which exhibits good chemical and electrochemical inertness under these conditions. If, on one hand, this setup allows fast screening, on the other, it is generally not representative of a practical device, where a gas diffusion electrode (GDE) can overcome the problem of low O_2 solubility in water. One of the main issues and a not well-documented aspect is the role of "support" in the electrochemical screening experiment. If GC is known to have low interference in RRDE measurements since it is generally well covered by a catalyst layer, in the GDE experiment, the intrinsic porosity of carbon paper or carbon cloth used for supporting the catalysts makes its exposure non-negligible. This is more evident in neutral or alkaline media, in particular when the catalyst loading is low (*ca.* 10^{-1} mg cm^{-2}); this is caused by the shift to an outer sphere electron transfer mechanism, which makes the role of the metal less central, in favour of the carbon matrix itself.[9] For these reasons, this work places particular emphasis on the effect of catalyst loading in GDE measurements to show how selectivity can be easily lost as the catalyst loading increases. For this purpose, we prepare two different catalysts featuring p-block metals, namely Sn (Sn-N-C) and Sb (Sb-N-C), with similar activity and different selectivity, to investigate the loading-dependent H_2O_2 selectivity loss, in particular in the GDE setup. The use of Sn and Sb was chosen not only to study unconventional metal centers,[10] but also to avoid the heterogeneous Fenton reaction, which has not been reported for these metal centers.[11] The effectiveness of single-atom catalysts based on Sn has been demonstrated both computationally[12] and practically, claiming both two-electron[13–15] and four-electron[16–18] ORR pathways. Similar to Sn, Sb is a low-toxicity, stable, and relatively abundant resource. The electron-rich nature of Sb provides a strong affinity for electron-deficient O_2 molecules, facilitating simple chemical reactions and electron transfer.[10] Also, in this case, there are several examples of Sb-based single-atom catalysts. For example, Wang *et al.* developed a p-block single-atom Sb catalyst featuring an Sb-N_4 coordination environment.[10,19]

Their study revealed that the p orbitals of Sb can efficiently interact with the p orbitals of oxygen, providing adequate adsorption strength for oxygen intermediates while reducing the reaction energy barrier. Also, for Sb, both four-electron[20–22]

University of Padova, Department of Chemical Science, Via Marzolo 1, Padova, 35131, Italy. E-mail: christian.durante@unipd.it

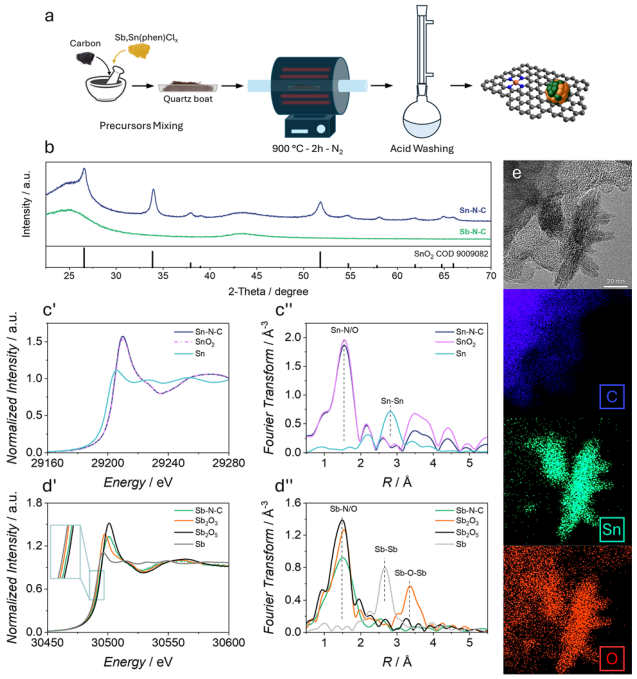

Fig. 1 (a) Synthetic pathway. (b) XRD of the two catalysts, with the SnO_2 phase reference for Sn-N-C. (c′) XANES region of Sn-N-C catalysts with Sn^0 and Sn^{4+} references. (c″) The FT of the EXAFS region. (d′) XANES region of Sb-N-C catalysts with Sb^0, Sb^{3+}, and Sb^{5+} references, (d″) FT of the EXAFS region, and (e) the STEM–EDX image of Sn-N-C.

and two-electron[23,24] catalysts have been reported. Here, Sn- and Sb-N-C catalysts were prepared using a two-step procedure as reported in Fig. 1a. The first step is pyrolysis of a mixture of a metal–phenanthroline complex and commercial Vulcan XC72 carbon black. This was carried out in an inert atmosphere (N_2) at 900 °C for 2 h. After this, the obtained powder was leached in 1 M H_2SO_4 for 3 h at 100 °C. This produces, in principle, a clean N-doped graphitic matrix with dispersion of single-site atoms (see the SI for details); instead, Sn and Sb exhibited two different behaviours. It is known from previous studies[15] that Sn forms metallic Sn during pyrolysis, which is then oxidized to SnO_2 during acid washing, as verified in this work (Sn-N-C 1T in Fig. S1). Also, in this study, the presence of SnO_2 was verified by XRD (Fig. 1b) and XAS (Fig. 1c) analyses. Indeed, this produces a catalyst, which is a mixture of SnN_x single-atom centers and SnO_2, which does not catalyze H_2O_2 decomposition (details are given below). The presence of SnN_x was confirmed by intensive washing[25] and XAS analysis (washed Sn-N-C 1T in Fig. S1), showing a decrease in the Sn–Sn signal of the oxide, as well as the disappearance of the SnO_2 signal in the XRD pattern (Fig. S1a). No further treatments were performed in order to simplify the synthesis and due to promising results in similar studies in neutral media.[15] Sb, on the other hand, does not produce any metallic phase during pyrolysis (Sb-N-C 1T in Fig. S1) and therefore in the final catalysts as well (XRD in Fig. 1b). In more detail, the XAS results reveal that all Sn is in the 4+ state, which is compatible with both SnN_x sites and SnO_2; in particular, this is clear from the superimposition of XANES spectra in Fig. 1c′ and from the absence of the Sn–Sn signal of metallic Sn in the EXAFS profile (Fig. 1c″). Also, the Sn–Sn component of the oxide is lower in the catalyst, suggesting the coexistence of the two species. This is further supported by the washed Sn-N-C catalyst, which still shows an XAS signal compatible with a 4+ oxidation state, but no XRD peak of the oxide is observed (Fig. S1). For Sb, the XANES signal lies between the Sb_2O_3 and Sb_2O_5 signals, corresponding to an oxidation state greater than 3+. This is in line with previous findings on Sb-N-C,[21] although lower oxidation states (<+3) have been reported elsewhere.[19,20,23] Finally, a STEM–EDX image of Sn-N-C was recorded to evaluate the morphology of SnO_2. As expected from the triangular-like XRD peaks (Fig. 1b), nanoparticles show irregular (non-spherical) shapes, as clearly evident from Fig. 1e, and a non-monodisperse dimensional distribution. The XRD peak width suggests a crystallite dimension of approximately 15 nm (from the Scherrer equation), which aligns with what was observed by TEM. Finally, the Fourier transform of a portion with nanoparticles (Fig. S2) shows spots that resemble the periodicity of SnO_2. The elemental map reveals the superimposition of Sn and O in the nanoparticle region, but at the same time, some Sn is also detected in the carbonaceous portion of the sample, corroborating the thesis on possible SnN_x functionalization. In conclusion, both catalysts are believed to contain single-site metal centers coordinated with nitrogen; in the case of Sn, these are accompanied by some SnO_2 particles. Following the chemical and physical characterization, a first test on the RRDE was performed. Each catalyst was drop-cast onto a GC disk-Pt ring electrode with a loading of 0.6 mg cm^{-2}. Linear sweep voltammetry (LSV) was conducted in 0.1 M KOH (pH = 13) between 1 and −0.4 V *vs.* RHE with a scan rate of 5 mV s^{-1} at 1600 rpm (Fig. 2a). For the collection of H_2O_2, practically HO_2^- at this pH, the ring potential was set to 1.5 V *vs.* RHE. As can be observed

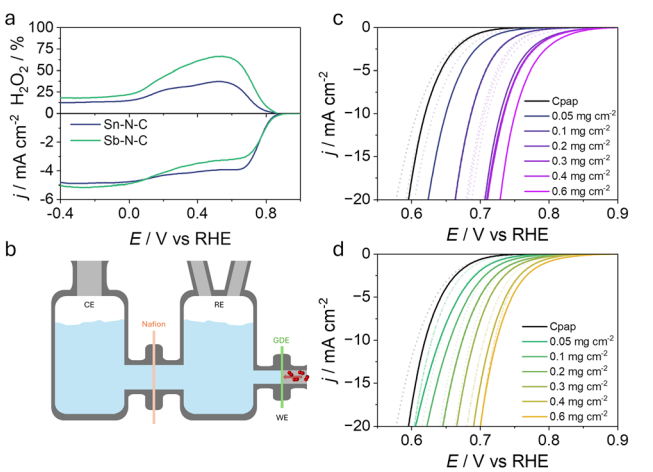

Fig. 2 (a) Linear sweep voltammetry and H_2O_2 yield of the two prepared catalysts (v = 5 mV s^{-1}, 1600 rpm, 0.1 M KOH (+ K_2SO_4 to improve conductivity), O_2-saturated; loading: 0.6 mg cm^{-2}). (b) Pictorial scheme of the GDE H-cell. (c) and (d) LSV in the GDE configuration for Sn-N-C (c) and Sb-N-C (d) at different tested loadings compared to the bare carbon paper support (Cpap). The cathodic compartment contains 0.1 M KOH (+ K_2SO_4). The LSV curve after 4 h is shown as a light colored dotted line.

from Fig. 2a, the Sb sample shows a higher faradaic efficiency peaking over 60%, while Sn-N-C reaches a maximum of 35%. It is also clear that these two catalysts show a 2-step reaction, between 0.8 and 0 V *vs.* RHE. The LSV curve reaches a first plateau current, which corresponds to the region where the selectivity reaches a peak. Then, between 0 and −0.4 V *vs.* RHE, the current reaches a slightly lower (higher in modulus) value, with selectivity stabilizing at the lower observed value along the entire LSV. This could imply a first region where O_2 is reduced to both H_2O_2 and H_2O and a second one where H_2O_2 is also reduced to H_2O. This behavior is common to both catalysts. Compared to bare glassy carbon, there is a clear difference in activity (Fig. S3a), proving catalytic activity. To better understand the role of SnO_2 in Sn-N-C, measurements on the sole oxide were carried out. Fig. S4a–c shows the RRDE response. SnO_2 is revealed to be similar in activity to bare glassy carbon (GC) with a low production rate of H_2O_2 despite good selectivity, higher than that of Sn-N-C. The selectivity drops to a lower value below 0.3 V *vs.* RHE. This excludes a possible effect of SnO_2 in catalysing the decomposition of H_2O_2 in the potential region where Sn-N-C and Sb-N-C show the biggest difference. This is also corroborated by a CV experiment with O_2 and H_2O_2.

In the presence of O_2, two distinct reduction peaks are observed (Fig. S4d). The peak at more negative potential is also observed with H_2O_2, which suggests that H_2O_2 is reduced at more negative potentials compared to O_2 and/or the mechanism varies below 0.3 V. The next step was to move to a GDE setup to close the gap with a practical device. For this purpose, an H-cell with an aperture to place a diffusion electrode (Fig. 2b) was used. This consists of two 150 mL chambers filled with electrolyte solution. On the counter electrode side, an acidic solution (pH 1) was used, while on the cathodic side, an alkaline solution (pH 13) was used. This was done to facilitate proton diffusion through the membrane by increasing the gradient. Materials were vacuum-filtered on carbon paper with a microporous carbon layer (MPL) at different loadings (all the experimental details are given in the SI). The first test was conducted at the same loading as that used for the RRDE, namely 0.6 mg cm^{-2}. The observed activity is in line with that of the RRDE (Fig. S3b) when the current is converted to pure kinetic current using the Koutecký–Levich equation. This is a very useful comparison that allows us to quickly understand whether shifting to a GDE causes any hindrance to the activity. To evaluate the selectivity (faradaic efficiency, FE), chronopotentiometry was performed by fixing the current at −5 mA cm^{-2} for 4 h. The solution was sampled at 30-minute intervals for evaluating H_2O_2 production using the Ti(IV) complexation method (see the SI for details). The GDE selectivity performance did not reach what was observed for the RRDE. Indeed, for Sn-N-C, the FE at a loading of 0.6 mg cm^{-2} is around 7.5% (Fig. 3b), which is lower than the maximum observed with the RRDE (Fig. 2a) and lower even when considering the same potential region (around 0.75 V) where chronopotentiometry was performed. The same is true for Sb-N-C, which reaches an FE of 21% (Fig. 3d), again lower than the peak observed for the RRDE (Fig. 2a) and in the same potential region where

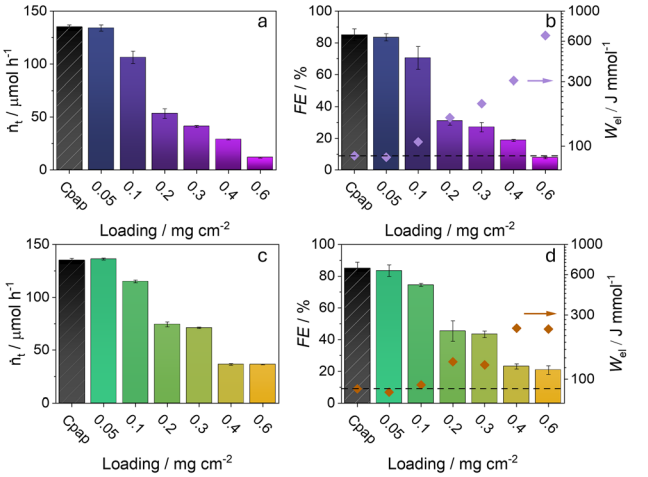

Fig. 3 H_2O_2 production rates of (a) Sn-N-C and (c) Sb-N-C evaluated as the slope of the linear fit between the produced amount at each sampling step, plotted against the catalyst loading. (b) and (d) The faradaic efficiency is plotted against the loading and reported together with the energy consumption for (b) Sn-N-C and (d) Sb-N-C.

chronopotentiometry was performed. When compared with the bare carbon paper (Cpap) used for supporting the material, the activity is clearly improved for both catalysts (Fig. 2c and d), although the advantage of having a catalyst layer is less pronounced compared to GC (Fig. S3a); in other words, the carbon paper with an MPL is more active than GC. In terms of selectivity, the opposite trend is observed. The bare carbon paper is observed to be more selective than the two catalysts, reaching an FE of over 80%. These relatively surprising results lay the basis for studying the effect of loading on GDE. The idea was to understand if there is a balance between activity (lower overpotential) and selectivity. Fig. 2c and d shows the variation of LSV curve as a function of the loading. For Sn-N-C (Fig. 2c), there is an initial important shift toward more positive potentials at loadings $\leq$0.1 mg cm^{-2}, followed by flattening between 0.2 and 0.6 mg cm^{-2}, possibly suggesting that not all the material is working efficiently or that the catalysts are not ideally homogeneous. From the production rate ($\dot{n}$), which is the number of moles produced per hour, it is clear that, being the current fixed, and therefore the charge, higher loading is detrimental to productivity (Fig. 3a). This is indeed true for selectivity, which decreases with increasing loading (Fig. 3b). The very same behavior is observed for Sb-N-C. The LSV (Fig. 2d) curve shifts toward a more positive potential, this time more "linearly" compared to Sn-N-C. The same trend is observed for the production rate ($\dot{n}$), except for 0.05 mg cm^{-2}, which was observed to be slightly more productive (Fig. 3c). The discrepancy between these results and the corresponding FEs is because the production rate is evaluated as a linear fit of concentration at each sampling point (every 30 minutes), while the faradaic efficiency is calculated at the end of chronopotentiometry.

This decrease in selectivity can be explained by considering both the growth of the catalyst layer and the slight positive shift of the working potential. It can be said that the residence time for a diffusing species is expected to increase with the square of

the layer thickness, which linearly scales with the loading. Consequently, H_2O_2 is more likely to encounter additional active sites, where it can undergo further reduction, particularly at N and metallic centers. Moreover, in the GDE configuration, the absence of forced convection limits product removal, although local alkalinization can promote electrostatic repulsion between HO_2^- and OH^-, thereby facilitating peroxide diffusion.[26] Also, under galvanostatic operation, the working potential is not directly controlled. The two investigated catalysts operate at more positive potentials than bare carbon paper, which actually works within a more favorable potential window for H_2O_2 selectivity. To support this interpretation, measurements were performed using only the carbon support (C) on both the RRDE and GDE at a loading of 0.6 mg cm^{-2} (Fig. S4). While C exhibited a comparable H_2O_2 production rate but lower activity on the RRDE, switching to the GDE configuration resulted in a production rate similar to that of Cpap. In this case, the behavior cannot be attributed to mass transport but to the lower working potential, which is beneficial for selectivity, and to the absence of highly active sites capable of further reducing H_2O_2. Discussing the RRDE/GDE discrepancy, the next step was to understand the feasibility of H_2O_2 production with the catalyst used. An energy consumption (electrochemical work, W_{el}) parameter was defined as a function of the overpotential, current, and the production rate, which is also related to FE (see the SI, S2.7). This gives the work normalized by the moles produced, whose magnitude is inversely proportional to the efficiency; lower values are given by the best combination of activity and selectivity. Dots in the secondary axes in Fig. 3c and d indicate the obtained values for all loadings and for Cpap. It reaches an energy consumption of 85 J $mmol^{-1}$, which is slightly higher than that of the two catalysts at 0.05 mg cm^{-2}. For Sn-N-C, the value is 83, while for Sb-N-C it is 80 J $mmol^{-1}$, which represents an improvement of approximately 6% compared to Cpap. An increase to a loading of 0.1 mg cm^{-2} results in a non-competitive value for Sn-N-C (109 J $mmol^{-1}$), while Sb-N-C is still close to bare carbon paper in performance (91 J $mmol^{-1}$). These results align with the better selectivity observed for Sb-N-C in the RRDE, but far from the expected H_2O_2 production rate. This is extremely evident at 0.6 mg cm^{-2}, where W_{el} reaches 660 J $mmol^{-1}$ for Sn-N-C and 236 J $mmol^{-1}$ for Sb-N-C. These results clearly show how important it is to carefully separate the activity and selectivity when a GDE is used, since trapping phenomena are amplified due to the absence of forced mixing in the proximity of the electrode, as is true for the RRDE. Also, fixing a current could cause a shift in potential and FE with loading affecting the work consumption.

In summary, Sn- and Sb-based catalysts were developed for H_2O_2 production *via* 2e-ORR in alkaline media. Catalyst loading strongly influenced performance: higher loadings increased activity but decreased selectivity. While bare carbon paper showed the highest selectivity, low loadings (<0.1 mg cm^{-2}) enhanced activity with little selectivity loss, likely by lowering overpotential without promoting further H_2O_2 reduction. These findings highlight the importance of optimizing support and loading in GDEs and demonstrate the usefulness of energy-consumption and K–L analyses for balancing efficiency and selectivity and comparing RRDE and GDE results.

Conflicts of interest

There are no conflicts to declare.

Data availability

The data supporting this article are included in the supplementary information (SI). Supplementary information: includes catalyst synthesis and characterization, RRDE and GDE experimental procedures, H_2O_2 quantification methods, electrochemical data analysis, and additional structural, spectroscopic, and electrochemical results supporting the findings of this study. See DOI: https://doi.org/10.1039/d6cc01757f.

Acknowledgements

Supported by MUR through PRIN 2022 PNRR (P2022WANKS – ECHO-EF). Experiments were performed at the SAMBA beamline, SOLEIL Synchrotron (France). The authors thank Andrea Zitolo and the SOLEIL staff.

References

1 B. K. Kundu, *et al.*, *Chem. Sci.*, 2024, **15**, 16424–16435.
2 Y. Wen, *et al.*, *Angew. Chem.*, 2022, **134**, e202205972.
3 S. Yang, *et al.*, *ACS Catal.*, 2018, **8**, 4064–4081.
4 A. Verdaguer-Casadevall, *et al.*, *Nano Lett.*, 2014, **14**, 1603–1608.
5 M. Mazzucato, *et al.*, *ACS Catal.*, 2024, **14**, 6369–6403.
6 G. Zuccante, *et al.*, *Mater. Renewable Sustainable Energy*, 2025, **14**, 58.
7 T. Okazaki, *et al.*, *ACS Sustainable Chem. Eng.*, 2024, **12**, 9856–9863.
8 S. Rojas-Carbonell, *et al.*, *ACS Catal.*, 2018, **8**, 3041–3053.
9 N. Ramaswamy, *et al.*, *J. Phys. Chem. C*, 2011, **115**, 18015–18026.
10 H. Liang, *et al.*, *Adv. Mater.*, 2025, **37**, e10356.
11 Y. Liu, *et al.*, *Chem. Eng. J.*, 2023, **466**, 143147.
12 Y. Zhang, *et al.*, *Molecules*, 2023, **28**, 5571.
13 Y. Gu, *et al.*, *Nat. Synth*, 2025, **4**, 614–621.
14 P. Xu, *et al.*, *Angew. Chem., Int. Ed.*, 2026, **65**, e23314.
15 L. Zhao, *et al.*, *ChemSusChem*, 2025, **18**, e202401758.
16 X. Fu, *et al.*, *Small*, 2026, **22**, e13912.
17 X. Lin, *et al.*, *Adv. Energy Mater.*, 2024, **14**, 2303740.
18 X. Wang, *et al.*, *J. Am. Chem. Soc.*, 2024, **146**, 21357–21366.
19 T. Wang, *et al.*, *Angew. Chem., Int. Ed.*, 2021, **60**, 21237–21241.
20 Y. Gu, *et al.*, *Angew. Chem.*, 2022, **134**, e202202200.
21 D. Zhang, *et al.*, *Chem. Eng. J.*, 2022, **439**, 135700.
22 Y. Zhang, *et al.*, *Nano Lett.*, 2024, **24**, 4291–4299.
23 M. Yan, *et al.*, *Adv. Mater.*, 2024, **36**, 2402963.
24 M. Yan, *et al.*, *Nat. Commun.*, 2023, **14**, 368.
25 M. Mazzucato, *et al.*, *ACS Appl. Mater. Interfaces*, 2022, **14**, 54635–54648.
26 L. Cui, *et al.*, *Nat. Commun.*, 2024, **15**, 10632.

